

Ternary Aligned Nanofibers of RGD Peptide-Displaying M13 Bacteriophage/PLGA/Graphene Oxide for Facilitated Myogenesis

Yong Cheol Shin^{1*}, Chuntae Kim^{2*}, Su-Jin Song³, Seungwon Jun³, Chang-Seok Kim³, Suck Won Hong³, Suong-Hyu Hyon⁴, Dong-Wook Han^{3,✉}, Jin-Woo Oh^{2,✉}

1. Research Center for Energy Convergence Technology, Pusan National University, Busan 46241, Republic of Korea
2. Department of Nanofusion Technology, College of Nanoscience & Nanotechnology, Pusan National University, Busan 46241, Republic of Korea
3. Department of Cogno-Mechatronics Engineering, College of Nanoscience & Nanotechnology, Pusan National University, Busan 46241, Republic of Korea
4. Center for Fiber and Textile Science, Kyoto Institute of Technology, Matsugasaki, Kyoto 606-8585, Japan

*Yong Cheol Shin and Chuntae Kim contributed equally to this work.

✉ Corresponding author: Professor Dong-Wook Han, Department of Optics and Mechatronics Engineering, BK21+ Nano-Integrated Cogno-Mechatronics Engineering, College of Nanoscience & Nanotechnology, Pusan National University, Busandaehak-ro 63beon-gil 2, Geumjeong-gu, Busan 46241, Republic of Korea. Tel: +82 51 510 7725; Fax: +82 51 514 2358. E-mail address: nanohan@pusan.ac.kr. and Professor Jin-Woo Oh, Department of Nanoenergy Engineering, College of Nanoscience & Nanotechnology, Pusan National University, Busandaehak-ro 63beon-gil 2, Geumjeong-gu, Busan 46241, Republic of Korea. Tel: +82 51 510 6123; Fax: +82 51 514 2358. E-mail address: ojw@pusan.ac.kr.

© Ivyspring International Publisher. This is an open access article distributed under the terms of the Creative Commons Attribution (CC BY-NC) license (<https://creativecommons.org/licenses/by-nc/4.0/>). See <http://ivyspring.com/terms> for full terms and conditions.

Received: 2017.08.18; Accepted: 2017.12.23; Published: 2018.02.15

Abstract

Recently, there have been tremendous efforts to develop the biofunctional scaffolds by incorporating various biochemical factors. In the present study, we fabricated poly(lactic-co-glycolic acid) (PLGA) nanofiber sheets decorated with graphene oxide (GO) and RGD peptide. The decoration of GO and RGD peptide was readily achieved by using RGD peptide-displaying M13 bacteriophage (RGD-M13 phage) and electrospinning. Furthermore, the aligned GO-decorated PLGA/RGD peptide (GO-PLGA/RGD) ternary nanofiber sheets were prepared by magnetic field-assisted electrospinning, and their potentials as bifunctional scaffolds for facilitating myogenesis were explored. We characterized the physicochemical and mechanical properties of the sheets by scanning electron microscopy, Raman spectroscopy, contact angle measurement, and tensile test. In addition, the C2C12 skeletal myoblasts were cultured on the aligned GO-PLGA/RGD nanofiber sheets, and their cellular behaviors, including initial attachment, proliferation and myogenic differentiation, were evaluated. Our results revealed that the GO-PLGA/RGD nanofiber sheets had suitable physicochemical and mechanical properties for supporting cell growth, and could significantly promote the spontaneous myogenic differentiation of C2C12 skeletal myoblasts. Moreover, it was revealed that the myogenic differentiation was further accelerated on the aligned GO-PLGA/RGD nanofiber sheets due to the synergistic effects of RGD peptide, GO and aligned nanofiber structure. Therefore, it is suggested that the aligned GO-PLGA/RGD ternary nanofiber sheets are one of the most promising approaches for facilitating myogenesis and promoting skeletal tissue regeneration.

Key words: poly(lactic-co-glycolic acid), graphene oxide, RGD peptide, M13 bacteriophage, magnetic field-assisted electrospinning, myogenesis.

Introduction

During the last decades, there have been tremendous efforts to develop the biofunctional scaffolds that can not only provide secure

microenvironments for cell growth, but can also promote cellular behaviors. As part of these efforts, many studies have suggested and designed various

types of tissue engineering scaffolds using a variety of biomaterials. Although the scaffold materials are always contingent upon the target tissues or cells, biocompatible polymer-based scaffolds have been most popularly studied for tissue engineering scaffolds. In particular, polymer-based scaffolds can be functionalized with diverse biochemical factors, such as growth factor, peptide and drug, to confer promoting effects on cellular behaviors [1-3]. It has been reported that the specific peptides can be functionalized into polymeric scaffolds, and improve cell adhesion and differentiation [1]. Various growth factors or drugs have been also widely employed to control or enhance cell growth and tissue regeneration by incorporating into polymer scaffolds [1-4]. However, there are issues to be considered before the applications of these approaches, although the biochemical factor-incorporated scaffolds have excellent biological and physiological activities. The incorporated biochemical factors should be compatible with basic structural materials for immobilizing within them. In addition, suitable techniques are needed to minimize the loss of biochemical factors in the preparation of scaffolds, and peptide or drug purification processes require much time and high cost. Hence, there are a number of efforts underway to address these issues.

The M13 bacteriophage (M13 phage) has merged as a novel organic building block in biomedical applications. M13 phage is a harmless filamentous virus that can express many desired peptides on their surfaces [5-7]. It is compactly covered by the 2,700 major coat proteins (pVIII), which can be genetically engineered to display numerous desired peptides, leads to allow the facile preparation of desired peptide assembly [8, 9]. In addition, desired peptide-displaying M13 phages can be simply and economically produced by infecting bacteria and mass amplification process. Therefore, M13 phage is one of the most promising candidates for physiological and biological active peptide applications, and many studies have been recently carried out to support and promote the cellular behaviors, including proliferation and differentiation, by expressing specific peptides on the surface of M13 phages [10, 11]. In the present study, we used RGD peptide-displaying M13 phage (RGD-M13 phage) as a novel building block for the facile preparation of biofunctional scaffolds to address the drawbacks of synthetic peptides. The RGD peptide, a tripeptide (Arg-Gly-Asp) found within extracellular matrix (ECM) proteins, plays a pivotal role in cell adhesion, proliferation and differentiation [12, 13]. The RGD peptide-enriched scaffolds can noticeably promote cell adhesion. Therefore, we decorated RGD peptides

into poly(lactic-co-glycolic acid) (PLGA), a biodegradable polymer, nanofibers by using RGD-M13 phages.

On the other hand, in addition to the biochemical factors, there have recently been enormous efforts to employ graphene-family nanomaterials in biomedical fields [14, 15]. Graphene oxide (GO), a type of graphene-family nanomaterials, is an oxidized form of graphene having many oxygen-containing surface groups, such as hydroxyl, carbonyl, epoxy, and carboxyl groups. Therefore, GO can specifically interact with various biomolecules. Moreover, GO has been shown to enhance myogenic differentiation as well as cellular behaviors [16, 17]. Hence, we fabricated GO-decorated PLGA/RGD peptide (GO-PLGA/RGD) ternary nanofiber sheets, and investigated their potentials as biofunctional tissue engineering scaffolds. Furthermore, the aligned GO-PLGA/RGD nanofiber sheets were prepared by magnetic field-assisted electrospinning (MFAES), and their effects on myogenesis were examined. In general, skeletal myoblasts differentiate into mature myotubes by fusion of neighboring cells, when they are fully proliferated. Therefore, myoblast alignment (i.e., end-to-end configuration) plays central role in cell fusion because skeletal myoblasts have spindle-like morphology. Additionally, it has been extensively acknowledged that the specific topographical cues of scaffold surface can directly induce the myoblast alignment, leads to the enhanced myogenic differentiation [18-22]. Herein, we explored the potentials of the aligned GO-PLGA/RGD ternary nanofiber sheets, which can provide both biochemical and surface topographical cues, for facilitating myogenesis.

Materials and Methods

Fabrication of aligned GO-PLGA/RGD ternary nanofiber sheets

The functionalization of RGD peptides into the electrospun fiber sheets was accomplished by utilizing RGD-M13 phages as reported in our previous studies [9, 23]. The RGD peptides were expressed on the side wall of M13 phage by genetic engineering. Briefly, an inverse polymerase chain reaction cloning method was conducted to express RGD peptides on major coat proteins of M13 phages, as describe elsewhere [9, 24, 25].

GO was synthesized from expanded graphite using a modified Hummers and Offeman method [26]. As a starting material, a small amount of expandable graphite (Asbury Carbon, Grade 1721) was placed into a 500 mL beaker and heated for ~10 s in a microwave oven; the expansion of graphite to ~150 times its original volume was induced. For the

acid treatment process, a 250 mL flask, equipped with a Teflon-coated magnetic stirrer, was filled with 50 mM of concentrated sulfuric acid. The flask was then placed into an ice bath maintained at 0 °C. Subsequently, the expanded graphite (2 g) was added slowly to the flask to make a suspension, followed by the slow addition of potassium permanganate (6 g). The temperature was then increased to 35 °C, and the suspension was stirred for approximately 2 h. The flask was then placed in an ice bath to cool the mixture, and the excess deionized water was added slowly to the mixture, maintaining the temperature below 70 °C. H₂O₂ (30 wt%) was then added slowly to remove the potassium permanganate; vigorous bubbles appeared and the color of the suspension changed from dark brownish to yellow. The suspension was filtered several times and diluted with deionized water to remove the acid completely; the pH of the dispersion was monitored until it reached 6. Finally, after suction drying over 12 h, the GO was prepared.

GO-PLGA/RGD ternary nanofiber sheets were produced by electrospinning technique. The electrospinning solution was prepared by dissolving PLGA (lactide/glycolide molar ratio = 75/25, molecular weight = 70,000–110,000 Da, 200 mg/mL, Evonik Industries, Essen, Germany) and RGD-M13 phages (10 mg/mL) in 1, 1, 1, 3, 3, 3-hexafluoro-2-propanol (Sigma-Aldrich Co., St Louis, MO, USA), and then GO solution (2 mg/mL, Sigma-Aldrich Co.) in water was blended with RGD-M13 phage and PLGA blend solution. Electrospinning was conducted by loading the RGD-M13 phage, GO and PLGA blend solution in a syringe attached to a 21-gauge needle. A voltage of 14 kV was applied and the blend solution was injected at a feeding rate of 0.2 mL/h. A steel rotating wheel covered by aluminum foil was placed 11 cm from the needle tip to collect the nanofibers. After then, GO-PLGA/RGD sheets were kept in vacuum for at least 8 h at room temperature in order to eliminate all remaining solvent.

The aligned GO-PLGA/RGD ternary nanofiber sheets were fabricated MFAES method at collector rotation speed of 2000 rpm. The MFAES is an effective technique for fabricating aligned fiber sheets by introducing an external magnetic field to the collector. The external magnetic field is introduced by a collector, where grounded and insulated regions are alternately placed. The aligned nanofiber sheets are fabricated by electrostatic interactions leading to the charged nanofibers to reach rotating collector and span across the gap between neighboring grounded regions [27-29].

Characterizations of aligned GO-PLGA/RGD ternary nanofiber sheets

Surface morphologies of electrospun nanofiber sheets were characterized by scanning electron microscopy (SEM; S-800, Hitach, Tokyo, Japan) with a 5 kV acceleration voltage. The sheets were coated with an ultrathin layer of gold/platinum by an ion sputterer (E1010, Hitach, Tokyo, Japan) prior to SEM observations.

The fast Fourier transform (FFT) method was presented for investigating the alignment of constituent nanofibers [30-33]. The information of optical data image is converted from a “real” domain to a mathematically defined ‘frequency’ domain by FFT function. The results of FFT output image is presented as grayscale pixels, and reflect the degree of fiber alignment in the original data image. The SEM images were analysis by FFT method using ImageJ software (National Institutes of Health, Bethesda, MD, USA) supported by an oval profile plug-in (created by William O’Connell). The FFT frequency distributions were created by placing an oval projection on the FFT image and radial summing of the pixel intensities for each angle between 0 and 360°. The pixel intensities were integrated between center and edge of images on each radius. Because FFT frequency distributions were symmetric, the pixel intensities were presented between 0 and 180°. All FFT data were normalized to compare data sets obtained in each experimental group (i.e. PLGA, GO-PLGA, PLGA/RGD, random GO-PLGA/RGD, and aligned GO-PLGA/RGD nanofiber sheets) by using ImageJ software. The normalized intensities represented electrospun fiber alignment in SEM images.

Water contact angles of the nanofiber sheets were measured to investigate the surface hydrophilicity of the sheets using a OCA10 goniometer (Dataphysics, Filderstadt, Germany) by placing a drop of distilled water (10 µL) on the nanofiber sheets.

The composition of electrospun nanofiber sheets was analyzed by Raman spectroscopy. The Raman spectra of nanofiber sheets were obtained by a Raman spectrometer (Micro Raman PL Mapping System, Dongwoo Optron Co., Kwangju, Korea) with excitation at 514.5 nm using an Ar-ion laser with a radiant power of 5 mW.

The mechanical properties of the nanofiber sheets were examined by obtaining the stress-strain curves of the sheets using a tabletop tensile tester (LRX Plus Series, Ametek Lloyd Instruments Ltd., Fareham, UK) equipped with a 5 kN load cell under a cross-head speed of 10 mm/min. Prior to testing, 5 types of sheets, including PLGA, GO-PLGA, PLGA/RGD, random GO-PLGA/RGD, and aligned

GO-PLGA/RGD nanofiber sheets, were cut into a rectangular shape, 40 mm in length and 10 mm in width. The aligned GO-PLGA/RGD nanofiber sheets were analyzed in longitudinal and transverse directions.

Cell Cultures and Conditions

The C2C12 mouse skeletal myoblasts were purchased from the American Type Culture Collection (Rockville, MD, USA) and routinely maintained in Dulbecco's modified Eagle's Medium (DMEM, Welgene, Daegu, Korea) supplemented with 10 % fetal bovine serum (Welgene) and a 1 % antibiotic-antimycotic solution (containing 10,000 units penicillin, 25 μ g amphotericin B and 10 mg streptomycin per mL, Sigma-Aldrich Co.) at 37 °C in a humidified atmosphere containing 5% CO₂.

In vitro assays for C2C12 myoblast behaviors on aligned GO-PLGA/RGD ternary nanofiber sheets

The *in vitro* biocompatibility of fabricated nanofiber sheets, including PLGA, GO-PLGA, PLGA/RGD, and GO-PLGA/RGD nanofiber sheets, was examined according to the ISO 10993 standards for evaluating the biocompatibility of medical devices. The detailed experimental conditions for biocompatibility assays were described in Supporting Information.

To examine the initial attachment and proliferation of C2C12 skeletal myoblasts on GO-PLGA/RGD nanofiber sheets, a cell counting kit-8 assay (CCK-8 assay, Dojindo, Kumamoto, Japan) was performed following the manufacturer's protocol. The number of viable cells was directly proportional to the metabolic reaction products obtained in the CCK-8 assay [34, 35]. Briefly, a concentration of 1×10^4 cells/mL was seeded on each sheet, and incubated for 4 h (initial cell attachment) or 1, 3, 5 and 7 days (proliferation) at 37 °C. After then, the cells were incubated with CCK-8 solution for another 2 h in the dark at 37 °C. The absorbance values were determined by using SpectraMax[®] 340 plate reader (Molecular Devices, Sunnyvale, CA, USA) at 450 nm. The relative cell viability was determined as the percentage of the optical density value in the cells to the optical density value of control groups. The absorbance values of the cells cultured on tissue culture plastics (TCPs) were used as positive controls.

Immunofluorescence staining analysis of myogenic differentiation on aligned GO-PLGA/RGD ternary nanofiber sheets

In order to evaluate the myogenic differentiation

of skeletal myoblasts on GO-PLGA/RGD ternary nanofiber sheets, C2C12 cells were seeded on PLGA, GO-PLGA, PLGA/RGD, random GO-PLGA/RGD, and aligned GO-PLGA/RGD nanofiber sheets at a density of 1×10^4 cells/mL, and incubated for 7 days. The myogenic differentiation of C2C12 skeletal myoblasts on the nanofiber sheets was examined by immunofluorescence staining for myogenin and myosin heavy chains (MHCs). The cells were fixed with formalin solution (3.7% of formaldehyde solution, Sigma-Aldrich Co.) for 10 min, permeabilized with 0.1% Triton X-100 (Sigma-Aldrich Co.) in Dulbecco's phosphate-buffered saline (DPBS, Gibco, Rockville, MD, USA) for 5 min and blocked with 2% bovine serum albumin (BSA, GenDEPOT, Barker, TX, USA) solution for 30 min. The myogenin was immunofluorescence stained with an anti-myogenin monoclonal antibody (clone F5D, 1:100 in 1% of BSA solution in DPBS; Santa Cruz Biotechnology Inc., Santa Cruz, CA, USA) for overnight at 4 °C, followed by a secondary Alexa Fluor 488-conjugated anti-mouse IgG (at 1:200 in 1% of BSA solution in DPBS; Molecular Probes, Eugene, OR, USA) for 1 h at room temperature. To immunofluorescence staining for MHCs, cells were incubated with the Alexa Fluor 488-conjugated anti-MHC monoclonal antibody (clone MF20, 1:200, eBioscience Inc., San Diego, CA, USA) overnight at 4 °C. F-actins were stained with the tetramethyl rhodamine isothiocyanate (TRITC)-labeled phalloidin (at 1:40 in 1% of BSA solution in DPBS; Molecular Probes) for 20 min in the dark at room temperature, and the nuclei were counter stained using 4',6-diamidino-2-phenylindole (DAPI, 1 μ M, Sigma-Aldrich Co.). The stained cells were imaged using a custom-built two-photon excitation fluorescence microscope [36, 37]. The immunofluorescence images were analysed using ImageJ software, and the myoblast alignment was examined as described in "**Characterizations of aligned GO-PLGA/RGD ternary nanofiber sheets**" section.

Statistical analysis

All variables were tested in three independent cultures for each experiment, which was repeated twice ($n = 6$). The quantitative data is expressed as the mean \pm standard deviation (SD). The data was tested for the homogeneity of the variances using the test of Levene, prior to statistical analysis. Statistical comparisons were carried out using a one-way analysis of variance (ANOVA; SAS Institute Inc., Cary, NC, USA), followed by a Bonferroni test for multiple comparisons. A value of $p < 0.05$ was considered statistically significant.

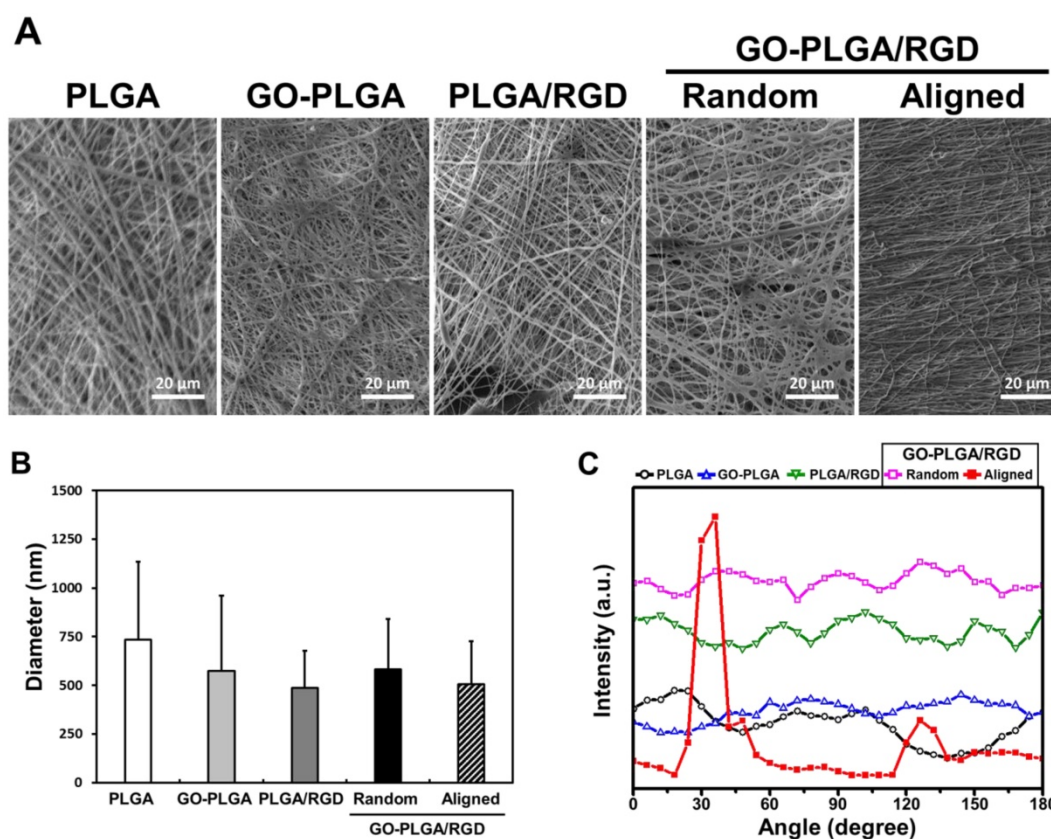


Figure 1. (A) Representative SEM images of PLGA, GO-PLGA, PLGA/RGD, random GO-PLGA/RGD, and aligned GO-PLGA/RGD nanofiber sheets. All images shown in this figure are representative of six independent experiments with similar results. (B) Average diameters of PLGA, GO-PLGA, PLGA/RGD, random GO-PLGA/RGD, and GO-PLGA/RGD nanofibers. (C) Pixel intensity plot of fiber alignment for PLGA, GO-PLGA, PLGA/RGD, random GO-PLGA/RGD, and aligned GO-PLGA/RGD nanofibers.

Results and Discussion

Characteristics of aligned GO-PLGA/RGD ternary nanofiber sheets

The surface morphology of the GO-PLGA/RGD ternary nanofiber sheets was shown to be a three-dimensional network structure resembling the natural ECM (Figure 1A). The average diameters were 735 ± 400 , 574 ± 386 , 485 ± 192 , 583 ± 258 , and 507 ± 221 nm for the PLGA, GO-PLGA, PLGA/RGD, random GO-PLGA/RGD, and aligned GO-PLGA/RGD nanofiber sheets, respectively (Figure 1B). The diameter of the fabricated nanofibers decreased when RGD-M13 phages and/or GO were blended (Figure 1A and 1B). It was reported that the diameter of the electrospun nanofibers was dependent on the properties of the electrospinning solution, such as viscosity, electrical conductivity, chemical composition, and molecular weight of the constituent polymers [38-40]. When RGD-M13 phage and/or GO suspensions were blended with PLGA solution, the electrical conductivity of the solution was increased due to the GO nanoparticles and the salts of the RGD-M13 phage suspension. In addition, the

viscosity of the electrospinning solution decreased with the blending of the RGD-M13 phage and/or GO suspensions. Therefore, the diameter of the GO-PLGA/RGD nanofibers decreased compared to that of the PLGA fibers. Regarding the surface area-to-volume ratio, this decrease in the diameter of the GO-PLGA/RGD nanofibers significantly increases the surface area-to-volume ratio of the sheets, which allows achieving effective interactions between the cells and GO-PLGA/RGD nanofiber sheets [41]. Therefore, the both random and aligned GO-PLGA/RGD nanofiber sheets can effectively interact with cells because of their superior surface area-to-volume ratio. Furthermore, the natural ECM is composed of various reticular fibers having diameters ranging from tens to hundreds of nanometers [42-44]. As shown in Figure 1B, the diameter of the GO-PLGA/RGD nanofibers widely varied in the range from 317 to 913 nm because the RGD-M13 phage and GO were randomly decorated into the PLGA fibers. Therefore, the GO-PLGA/RGD sheets composed of constituent fibers, which had various fiber diameters, were quite similar to the natural ECM in structural aspects. On the other hand, the aligned GO-PLGA/RGD nanofiber sheets were highly

aligned in a single direction. In addition, according to the SEM images presented in Figure 1A, there were no significant differences in the morphological properties between the aligned GO-PLGA/RGD nanofibers and other nanofibers. The aligned GO-PLGA/RGD nanofibers showed smooth, beadless and continuous morphologies, indicating that the MFAES was suitable technique for fabricating aligned nanofiber sheets. To analyze the degree of fiber alignment, FFT analysis was employed, and the pixel intensity in FFT frequency distribution reflects the degree of fiber alignment (Figure 1C). The aligned GO-PLGA/RGD nanofibers showed the dominant distribution near 30°, whereas random fiber sheets displayed a broad distribution of fiber angle. These results indicated that the aligned GO-PLGA/RGD nanofibers were successfully fabricated by MFAES.

Table 1. Water contact angles of PLGA, GO-PLGA, PLGA/RGD, random GO-PLGA/RGD, and aligned GO-PLGA/RGD nanofiber sheets.

Sample	Water Contact Angle (°)
PLGA	137.6 ± 2.0
GO-PLGA	120.6 ± 2.3
PLGA/RGD	83.8 ± 3.4
Random GO-PLGA/RGD	78.0 ± 2.8
Aligned GO-PLGA/RGD	90.0 ± 3.3

The data are expressed as the average ± standard deviation (SD) of at least three independent experiments, each performed in duplicate on different samples.

We measured the contact angles of sheets, because the surface hydrophilicity is one of the main factors that contributes to the interaction between cells and substrates (Table 1). The contact angles of the PLGA, GO-PLGA, PLGA/RGD, random GO-PLGA/RGD, and aligned GO-PLGA/RGD nanofiber sheets were 137.6 ± 2.0°, 120.6 ± 2.3°, 83.8 ± 3.4°, 78.0 ± 2.8°, and 90.0 ± 3.3°, respectively. Contact angles of the nanofiber sheets gradually decreased when GO was decorated in the nanofibers. This could be attributed to the abundant hydrophilic groups on the GO surface, such as hydroxyl, carbonyl and carboxyl groups [45]. In addition, the contact angles further decreased when RGD-M13 phage was incorporated in the nanofibers. Therefore, the GO-PLGA/RGD nanofiber sheets have the most hydrophilic surface among other matrices. The contact angle of aligned GO-PLGA/RGD nanofiber sheets was slightly increased compared to that of the random one, which was attributed to the fact that the aligned GO-PLGA/RGD sheets had smaller pore size than random sheets due to fiber alignment [46]. However, as compared to the PLGA and GO-PLGA nanofiber sheets, the aligned GO-PLGA/RGD nanofiber sheets possessed greatly hydrophilic surface. This increase in surface hydrophilicity of matrices can also

substantially facilitate the interactions between cells and matrices. Therefore, the GO-PLGA/RGD nanofiber sheets have suitable surface hydrophilic properties that can provide a favorable microenvironment for the cell adhesion and growth. The Raman spectroscopy was carried out to confirm the successful decoration of GO and RGD-M13 phages. Figure 2A showed the Raman spectra of PLGA, GO, RGD-M13 phage, and aligned GO-PLGA/RGD nanofiber sheets. In the aligned GO-PLGA/RGD nanofiber sheets, characteristic bands of PLGA were observed near 850 and 1760 cm⁻¹, which were assigned to the C-COO⁻ vibration of lactic acid and C=O stretching of the ester groups, respectively [47-49]. On the other hand, the noticeable D and G bands of GO were clearly observed at 1350 and 1600 cm⁻¹, respectively [50]. In addition, the specific bands near 950 and 1450 cm⁻¹ were found, which could be attributed to the C-COO⁻ stretching from carboxylate group of glycine and the CO₂⁻ stretching of a symmetric carboxylic acid, respectively [51, 52]. These results demonstrated that the aligned GO-PLGA/RGD nanofiber sheets were successfully fabricated by MFAES as well as GO and RGD-M13 phage were well decorated in the PLGA fibers.

Table 2. Mechanical properties (tensile strength, elastic modulus and ultimate strain) of PLGA, GO-PLGA, PLGA/RGD, random GO-PLGA/RGD, and aligned GO-PLGA/RGD nanofiber sheets. The aligned GO-PLGA/RGD nanofiber sheets were analyzed in longitudinal and transverse directions

Sample	Tensile Strength (MPa)	Elastic Modulus (MPa)	Ultimate Strain (%)
PLGA	5.31 ± 0.19	201.61 ± 40.75	220.73 ± 15.51
GO-PLGA	11.42 ± 0.62	386.20 ± 81.18	16.59 ± 1.17
PLGA/RGD	1.37 ± 0.27	45.35 ± 7.38	54.01 ± 5.39
Random GO-PLGA/RGD	4.55 ± 0.45	169.78 ± 26.31	6.79 ± 0.44
Aligned GO-PLGA/RGD in TD*	2.00 ± 0.51	157.38 ± 7.38	10.84 ± 1.31
Aligned GO-PLGA/RGD in LD**	10.98 ± 2.07	101.91 ± 17.88	23.67 ± 3.16

*TD: transverse direction; **LD: longitudinal direction

To investigate the mechanical properties of aligned matrices, tensile test was performed under a tensile load. The stress-strain curves of matrices were shown in Figure 2B. In addition, the tensile strength, elastic modulus and ultimate strain were obtained from the stress-strain curves of the matrices, and described in Table 2. The tensile strengths of the PLGA, GO-PLGA, PLGA/RGD, and random GO-PLGA/RGD nanofiber sheets were approximately 5.31, 11.42, 1.37, and 4.55 MPa, respectively (Figure 2B and Table 2). The elastic moduli of the PLGA, GO-PLGA, PLGA/RGD, and random GO-PLGA/RGD nanofiber sheets were about 201.61, 386.20,

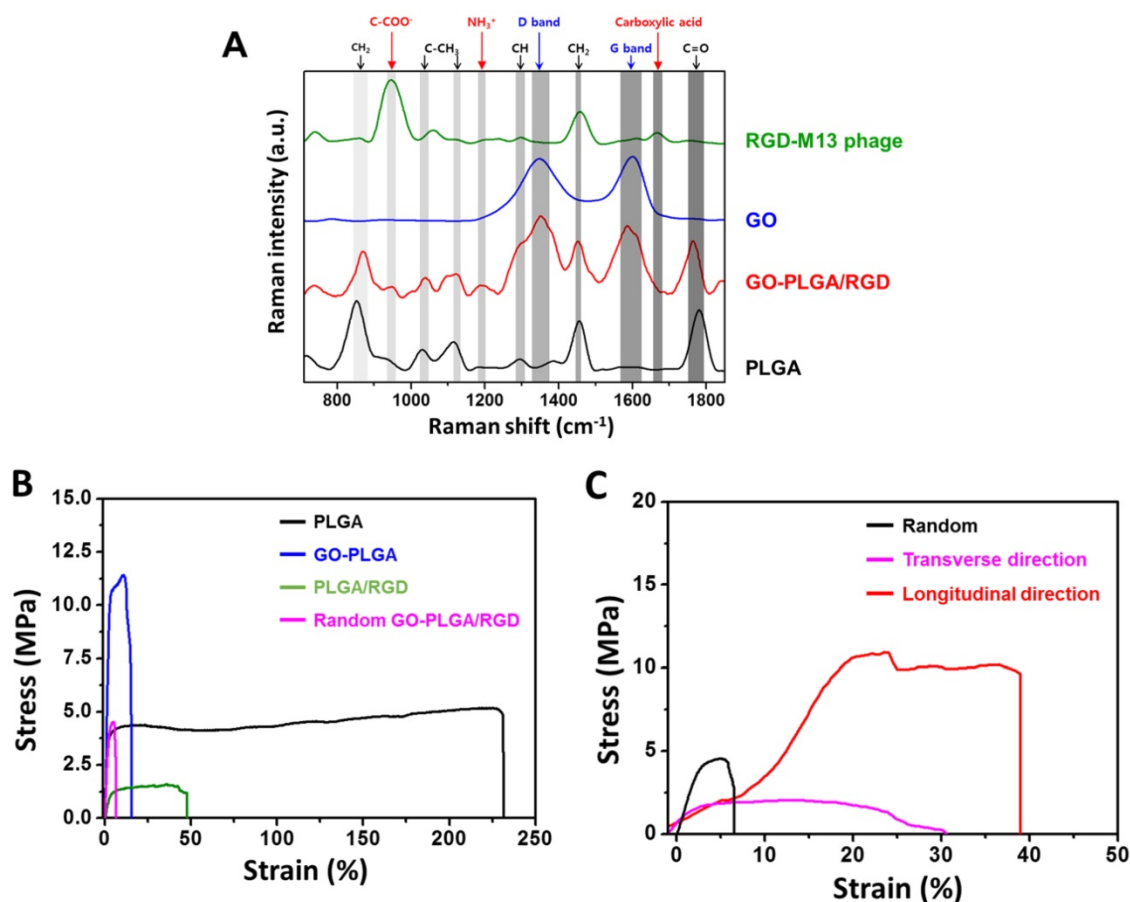


Figure 2. (A) Raman spectra of PLGA, GO, RGD-M13 phage, and GO-PLGA/RGD nanofiber sheets. (B) Stress–strain curves of the PLGA, GO-PLGA, PLGA/RGD, and random GO-PLGA/RGD nanofiber sheets under a cross-head speed of 10 mm/min. (C) Comparison of mechanical properties between random and aligned GO-PLGA/RGD nanofiber sheets.

45.35, and 169.78 MPa, respectively. The elastic moduli were obtained as the maximum linear slope of the stress–strain curve in the elastic deformation region [53, 54]. When RGD-M13 phages were blended into the sheets, the tensile strength and elastic modulus of sheets were decreased owing to their intrinsic poor mechanical properties. However, when GO was incorporated, the tensile strength and elastic modulus of matrices were significantly ($p < 0.05$) increased. This improved mechanical properties of matrices can be attributed to the incorporation of GO.

It has been noted that the GO can strongly interact with polymer matrix through chemical bonding between the oxygen-containing functional groups (e.g., hydroxyl, carbonyl, carboxyl, and epoxy groups) of the GO and the hydroxyl groups of the PLGA [55]. In addition, GO can also interact with the amino acids and carboxyl groups of the RGD-M13 phage. Therefore, the mechanical properties of GO-PLGA/RGD nanofiber sheets were remarkably reinforced due to the strong interfacial interactions between GO, PLGA and RGD-M13 phage. On the other hand, previous studies have shown that the attachment and proliferation of cells were markedly

influenced by the mechanical properties of substrates. Hence, these results suggest that the decreased mechanical properties owing to the functionalized RGD-M13 phages can be reinforced through the decoration of GO, and the GO-PLGA/RGD nanofiber sheets are able to serve as mechanically stable substrates for cell growth. On the other hand, the mechanical properties of fibrous substrates are highly dependent on the orientation and alignment of constituent fibers [18, 19]. Therefore, we compared the mechanical properties of random and aligned GO-PLGA/RGD nanofiber sheets. As shown in Figure 2C and Table 2, both fiber alignment and the direction of applied tensile stress had great effects on the tensile strength, elastic modulus and ultimate strain of sheets. When the tensile stress was applied in the longitudinal direction, the tensile strength and ultimate strain of the aligned GO-PLGA/RGD sheets were significantly increased as compared to the random matrices. On the contrary, the mechanical properties of the aligned sheets were found to be decreased when the tensile stress was applied in the transverse direction, even compared to random GO-PLGA/RGD sheets. These results are in complete

accordance with previous reports [18, 19, 56]. These alignment-dependent mechanical responses of substrates are significant factors that can guide and direct cellular behaviors. We therefore hypothesized that the aligned GO-PLGA/RGD nanofiber sheets can not only guide the alignment of myoblasts, but can also stimulate the spontaneous myogenic differentiation. To test our hypothesis, we cultured the C2C12 myoblasts on GO-PLGA/RGD nanofiber sheets, and investigated their cellular behaviors, such as attachment, proliferation and myogenic differentiation.

Cell growth of C2C12 skeletal myoblasts on aligned GO-PLGA/RGD ternary nanofiber sheets

Prior to examining the cell growth of C2C12 skeletal myoblasts on aligned GO-PLGA/RGD ternary nanofiber sheets, the biocompatibility of fabricated nanofiber sheets were assessed according to the ISO 10993 standards for evaluating the biocompatibility of medical devices (Figure S1) [57-59]. As shown in Figure S1, there were no significant differences in the cell viability between experimental groups. In accordance with ISO 10993-5, it should be noted that the cell viability less than 70% is considered cytotoxic. However, the cell viability of all groups was found to be higher than 90%. Hence, it was demonstrated that the fabricated nanofiber sheets were biocompatible for C2C12 skeletal myoblasts. To evaluate the cellular behaviors of C2C12 skeletal myoblasts on the aligned GO-PLGA/RGD ternary nanofiber sheets, we cultured C2C12 skeletal myoblasts on the sheets, and investigated their initial attachment and proliferation (Figure 3). As shown in Figure 3A, the initial attachment of C2C12 myoblasts was significantly ($p < 0.05$) increased on RGD peptide-containing sheets (i.e. PLGA/RGD, random

GO-PLGA/RGD and aligned GO-PLGA/RGD sheets) than that on control (TCPs), PLGA and GO-PLGA nanofiber sheets. It has been extensively known that the RGD peptides play a fundamental role in cell attachment, and the RGD peptide-enriched substrates can stimulate the cell attachment [12, 13, 60-62]. Therefore, the initial attachment of C2C12 skeletal myoblasts was exceptionally increased on the RGD peptide-containing sheets. Moreover, the proliferations of C2C12 myoblasts on the PLGA/RGD, random GO-PLGA/RGD and aligned GO-PLGA/RGD nanofiber sheets were significantly ($p < 0.05$) enhanced (Figure 3B). These enhanced cellular behaviors were attributed to the synergistic effects of RGD peptide and GO. According to the previous studies, the RGD peptide-enriched substrates are highly beneficial to both cell adhesion and proliferation since they can robustly activate the integrin-mediated signaling pathway [61, 63]; meanwhile GO also participated in the enhanced cellular behaviors by adsorbing serum proteins in culture media through electrostatic interactions between the serum proteins and oxygen-containing surface functional groups of GO, results in promoted cellular behaviors [16, 64, 65]. These synergistic effects of RGD peptide and GO can thus promote the growth of C2C12 myoblasts. In addition, considering the physicochemical properties of GO-PLGA/RGD sheets, the specific high surface area-to-volume ratio and surface hydrophilicity could also participated in facilitating the interactions between cells and matrices, leads to the enhanced attachment and proliferation of C2C12 myoblasts [66-68]. These findings indicated that the GO-PLGA/RGD nanofiber sheets were not only highly biocompatible, but could also promote the initial attachment and proliferation. On the other hand, interestingly, the proliferation rates of C2C12 myoblasts on random and aligned

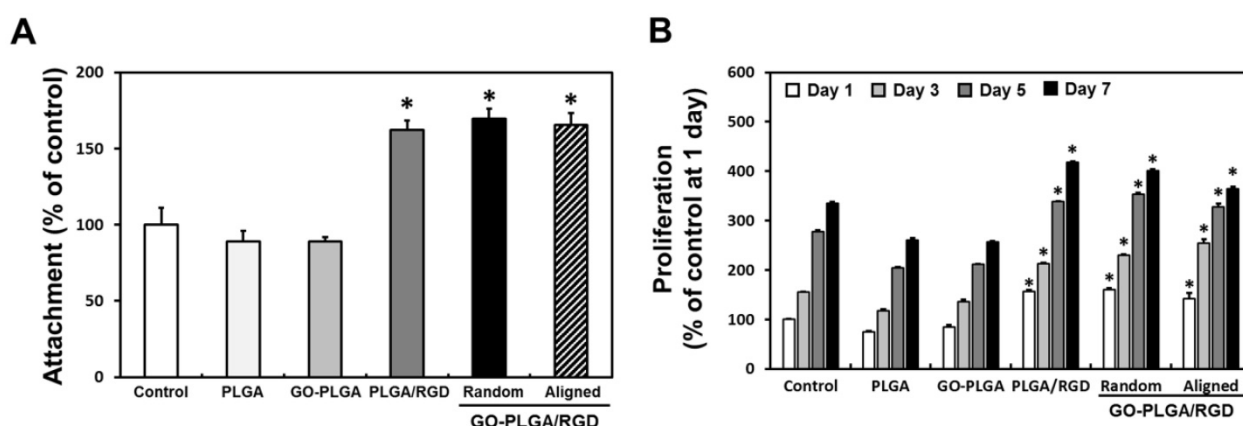


Figure 3. (A) Initial attachment and (B) proliferation of C2C12 skeletal myoblasts on the control (TCPs), PLGA, GO-PLGA, PLGA/RGD, random GO-PLGA/RGD, and aligned GO-PLGA/RGD nanofiber sheets. An asterisk (*) denotes a significant difference compared with the control ($p < 0.05$). The data are presented as the average \pm SD of at least three independent experiments, each performed in duplicate on different cultures.

GO-PLGA/RGD nanofiber sheets were slightly decreased at day 7. In general, skeletal myoblasts begin to fuse between neighboring cells, and to differentiate into mature myotubes rather than further proliferate, when they are sufficiently grown until intercellular contacts are occurred [69, 70]. We therefore speculated that the GO-PLGA/RGD sheets could stimulate and promote spontaneous myogenic differentiation of C2C12 myoblasts by the synergistic effects of RGD peptide and GO.

Facilitated myogenesis on aligned GO-PLGA/RGD ternary nanofiber sheets

To test our hypothesis, the C2C12 myoblasts were cultured on PLGA, GO-PLGA, PLGA/RGD, random GO-PLGA/RGD and aligned GO-PLGA/RGD nanofiber sheets for 7 days in growth media, and their myogenic differentiation was investigated by immunofluorescence staining for myogenin and

MHCs (Figure 4). The myogenin is an early stage marker of myogenic differentiation and a muscle-specific transcription factor that can induce myogenesis [16, 71, 72]. C2C12 myoblasts on the PLGA sheets showed abnormal morphology and much cellular debris owing to the intrinsic hydrophobic surface property of PLGA (Figure 4A). Additionally, the green fluorescence from myogenin was not observed. On the other hand, cells on the PLGA/RGD sheets were well grown, and the number of cells was appreciably increased as compared with that on PLGA sheets. However, the green fluorescence could also not be seen in the nucleus. In contrast, C2C12 myoblasts on GO-PLGA and GO-PLGA/RGD nanofiber sheets were not only favorably grown, but also exhibited green fluorescence from myogenin. In particular, on GO-PLGA/RGD sheets, strong green fluorescence was clearly detected. The percentage of myogenin-

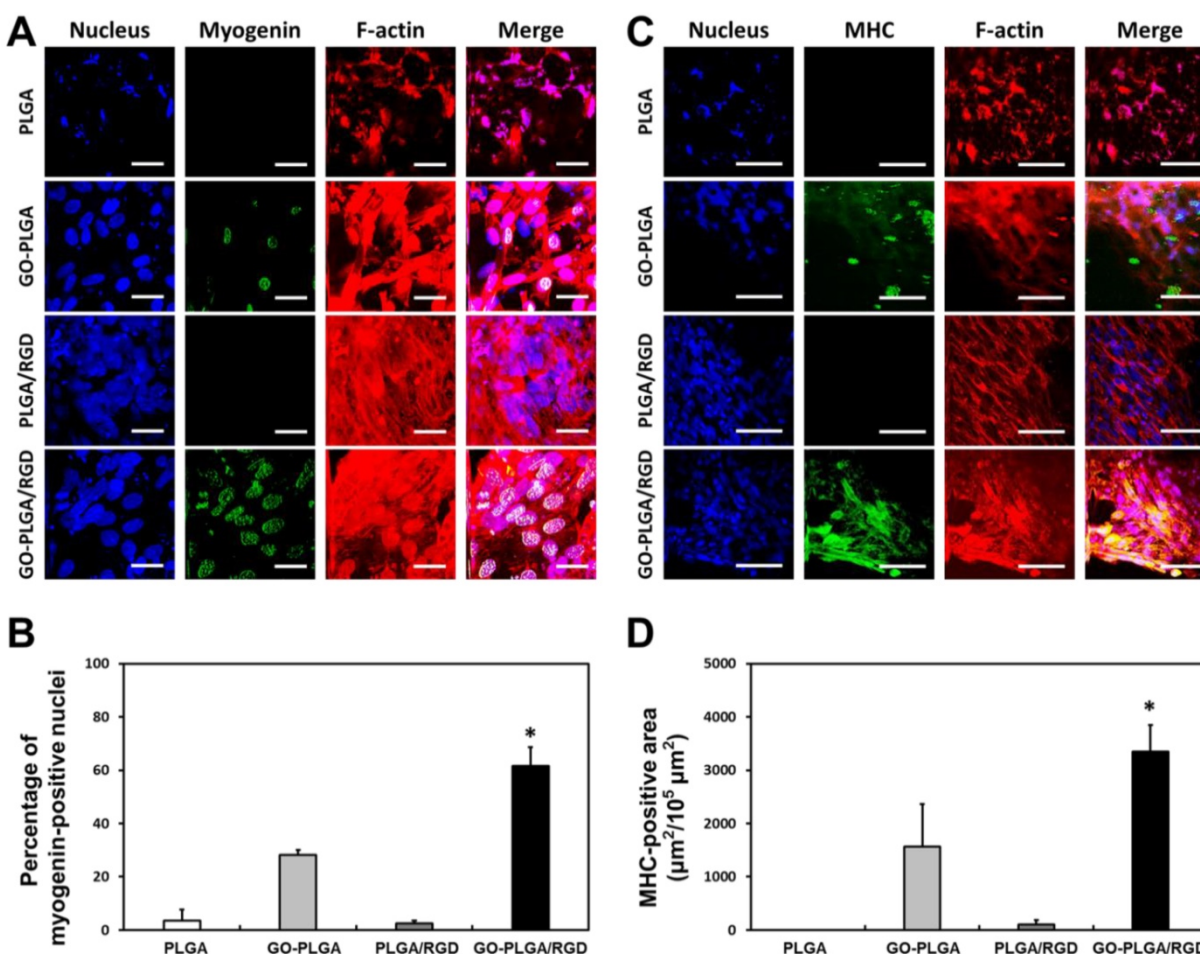


Figure 4. Immunofluorescence analysis for facilitated myogenesis of C2C12 skeletal myoblasts on PLGA, GO-PLGA, PLGA/RGD, and random GO-PLGA/RGD nanofiber sheets. **(A)** Two-photon excitation fluorescence images of C2C12 skeletal myoblasts stained with myogenin. The myogenin was stained with an anti-myogenin monoclonal antibody and a secondary Alexa Fluor 488-conjugated anti-mouse IgG (green). The scale bars are 25 μm . **(B)** Quantitative analysis of the percentage of myogenin-positive nuclei. **(C)** Two-photon excitation fluorescence images of C2C12 skeletal myoblasts stained with myosin heavy chains (MHCs). The MHCs were stained with Alexa Fluor 488-conjugated anti-MHC monoclonal antibody (green). The scale bars are 50 μm . **(D)** Quantification of MHC-positive area of C2C12 skeletal myoblasts. The cell nuclei were counterstained with DAPI (blue), the F-actins were stained with TRITC-labelled phalloidin (red). An asterisk (*) denotes a significant difference compared with the other groups ($p < 0.05$). The data are presented as the average \pm SD of at least three independent experiments, each performed in duplicate on different cultures.

positive nuclei was much higher on the GO-PLGA/RGD sheets than other groups (3.6% for PLGA, 28.2% for GO-PLGA, 2.5% for PLGA/RGD, and 61.6% for GO-PLGA/RGD sheets, respectively), implying that the GO-PLGA/RGD nanofiber sheets can stimulate the myogenic differentiation. To further examine the stimulating effects of GO-PLGA/RGD nanofiber sheets on the myogenic differentiation of C2C12 skeletal myoblasts, immunofluorescence staining for MHCs, a late stage marker of myogenic differentiation, was conducted, and the results are presented in Figure 4C and 4D. As shown in Figure 4C, the cells on the PLGA sheets could not be successfully grown and showed poorly-organized F-actins. However, on the PLGA/RGD and GO-PLGA/RGD nanofiber sheets, cells were successfully grown on the entire surface of matrices, and organized the network structure composed of well-developed F-actins (Figure 4C). On the other hand, the green fluorescence of MHCs was not exhibited from C2C12 myoblasts on PLGA and PLGA/RGD sheets, while the green fluorescence was detected from the cells on the GO-PLGA and, especially, GO-PLGA/RGD nanofiber sheets. These results indicated that the C2C12 myoblasts were fully proliferated on the GO-PLGA/RGD nanofiber sheets, followed by overt myogenic differentiation. The MHC-positive area ($\mu\text{m}^2/10^5 \mu\text{m}^2$) was measured to quantitatively compare the MHC expression in C2C12 skeletal myoblasts on nanofiber sheets (Figure 4D). The C2C12 skeletal myoblasts on the GO-PLGA/RGD nanofiber sheets exhibited remarkably high MHC-positive area. These results are in accordance with the earlier studies. It has been documented that the graphene and GO can enhance the differentiation of myoblasts, as well as various types of stem cells, such as mesenchymal, neural, embryonic, and induced pluripotent stem cells [16, 73-77]. In particular, GO has been found to stimulate and accelerate the myogenic differentiation of C2C12 myoblasts through increasing serum protein adsorption from culture media via interfacial interactions between serum proteins and the oxygen-containing functional moieties of the GO [16]. Hence, the GO-PLGA/RGD nanofiber sheets could significantly accelerated spontaneous myoblast fusion as well as the myotube maturation of myoblasts. As shown in Figure 4C, the well-formed and mature myotubes were evidently observed on the GO-PLGA/RGD nanofiber sheets. These findings strongly support our hypothesis that the GO-PLGA/RGD nanofiber sheets can not only promote cell adhesion and proliferation, but can also stimulate and accelerate the spontaneous myogenic differentiation. Therefore, the GO-PLGA/RGD nanofiber sheets are verified to be biofunctional

scaffolds that can stimulate and accelerate skeletal muscle differentiation as well as improve cellular behaviors.

According to the currently available literature, myoblast alignment is a critical factor in initiating and stimulating myogenic differentiation [19-21, 78]. In particular, the cell configuration plays an important role in fusion of myoblasts, and the end-to-end configuration of myoblasts can greatly enhance their fusion and myotube formation during early myogenic differentiation [79-82]. Therefore, to extend our findings for guiding C2C12 myoblast alignment, the myogenic differentiation of C2C12 skeletal myoblasts on the aligned GO-PLGA/RGD nanofiber sheets was examined. The C2C12 myoblasts were cultured on the aligned GO-PLGA/RGD nanofiber sheets in growth media for 3 and 7 days, and their behaviors were investigated (Figure 5). As shown in Figure 5A, the C2C12 myoblasts were well grown, and they began to orient themselves along the direction of the aligned nanofibers at 3 days after culture. The F-actins, especially, developed parallel to the aligned nanofiber direction (yellow arrows). However, C2C12 myoblasts could not yet be differentiated into myotubes and the green fluorescence of MHCs was not detected because they did not sufficiently proliferate to contact neighboring cells. Nonetheless, cells that began to align along the direction of nanofiber were clearly identified. After further culture for 4 days (total incubation time was 7 days), the myoblast alignment was obviously observed according to the direction of aligned fibers (Figure 5B). Moreover, the noticeable green fluorescence of MHCs was exhibited from the myoblasts. These results revealed that the aligned GO-PLGA/RGD nanofiber sheets can effectively induce myoblast alignment, and stimulate myogenic differentiation by facilitating myoblast fusion. It has been reported that the surface topographical cues are a major driving force for cell alignment [18, 22, 83]. To quantify the cell alignment, the angles between the F-actins and pre-determined axis were analyzed by FFT methods. As shown in Figure 5C, the angle distributions of F-actin direction on aligned GO-PLGA/RGD nanofiber sheets were most dominant at a specific degree: 24° for day 3 and 42° for day 7. On the contrary, the cells on the random GO-PLGA/RGD nanofiber sheets were randomly oriented, and the angles between the F-actins and pre-determined axis appeared relatively broad distribution (Figure 5C). In addition, the myoblast alignment ratio was substantially increased on the aligned GO-PLGA/RGD nanofiber sheets (Figure S2). In Figure S2, the angle of 0° corresponded to parallel alignment from the direction of aligned nanofibers

and the main axis of myoblasts, and the absolute angle of 90° denoted perpendicular alignment. The cells having an angle deviation less than 20° (i.e. $-10^\circ < \text{angle} < 10^\circ$) were estimated to be 23% for random GO-PLGA/RGD nanofiber sheets at day 7 (Figure S2A), 45.6% for aligned GO-PLGA/RGD nanofiber sheets at day 3 (Figure S2B) and 38.1% for aligned GO-PLGA/RGD nanofiber sheets at day 7 (Figure S2C), indicating that the myoblasts on the aligned GO-PLGA/RGD nanofiber sheets were highly aligned along the direction of aligned nanofibers. These results are largely consistent with previous reports, in which the aligned nanofiber matrices can directly induce cell alignment [20, 21, 78]. Moreover,

the C2C12 skeletal myoblasts on the aligned GO-PLGA/RGD nanofiber sheets exhibited apparently strong green fluorescence of MHCs as compare to those on the random GO-PLGA/RGD nanofiber sheets (Figure 4C and 5B). These results indicated that the aligned nanofiber sheets can further facilitate and accelerate the myogenic differentiation of myoblasts. Hence, our fascinating results suggest that the aligned GO-PLGA/RGD nanofiber sheets readily induce myoblast alignment as well as directly stimulate the myogenic differentiation by providing specific topographical guidance and biochemical cues, provided by the synergistic effects of RGD peptide, GO and aligned nanofiber structure.

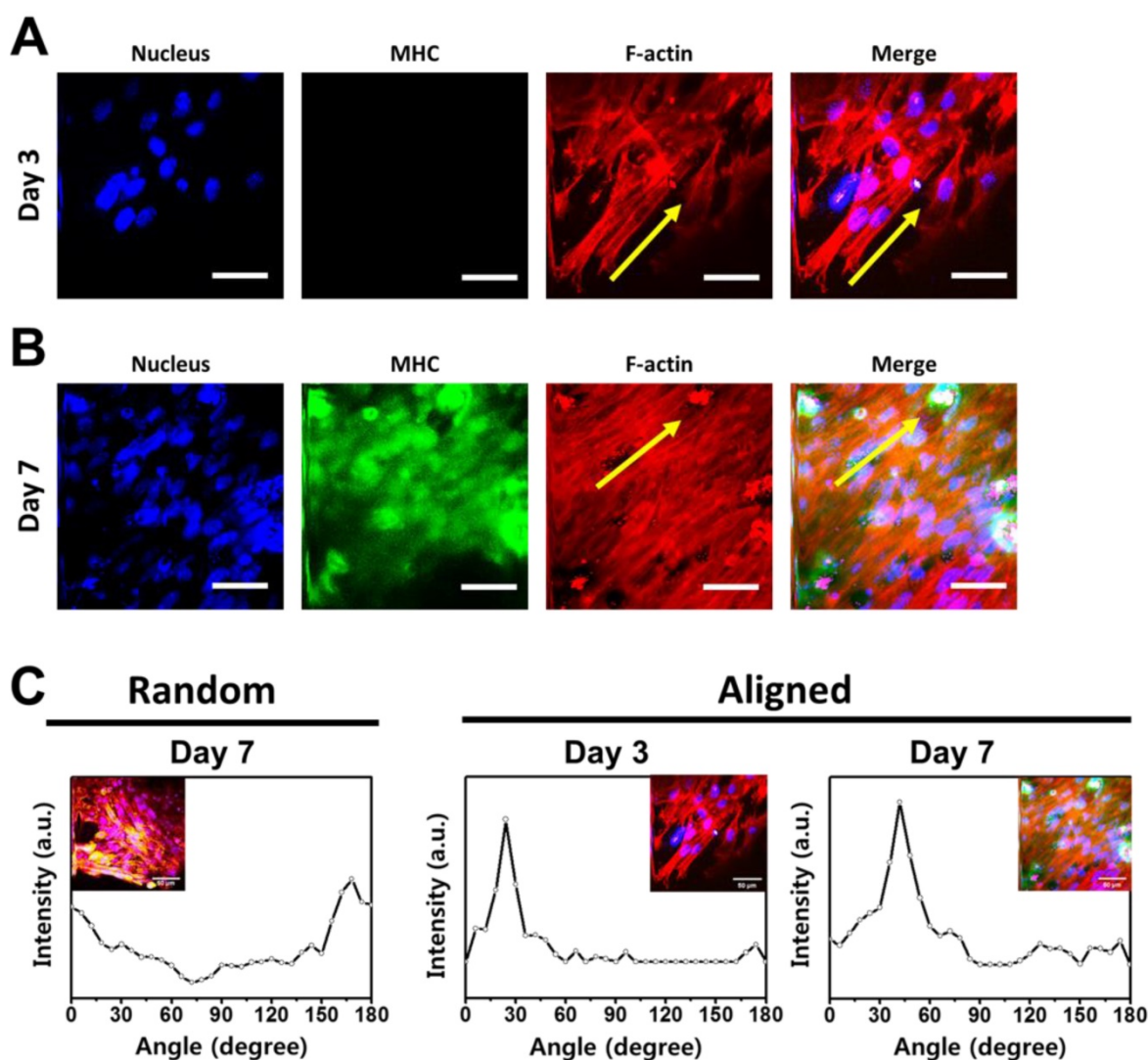


Figure 5. Immunofluorescence staining analysis of myogenic differentiation and myoblast alignment on the aligned GO-PLGA/RGD nanofiber sheets. **(A, B)** Two-photon excitation fluorescence images of C2C12 skeletal myoblasts on the aligned GO-PLGA/RGD nanofiber sheets at **(A)** 3 and **(B)** 7 days of incubation. The cell nuclei were counterstained by DAPI (blue), F-actins were stained with TRITC-labelled phalloidin (red) and the myosin heavy chains (MHCs) were stained with Alexa Fluor 488-conjugated anti-MHC monoclonal antibody (green). The scale bars are $50\ \mu\text{m}$. Yellow arrows indicate the direction of aligned nanofibers. All photographs shown in this figure are representative of six independent experiments with similar results. **(C)** Quantitative analysis of the cell alignment on the random and aligned GO-PLGA/RGD nanofiber sheets. Note the distinctive pixel intensity created by the FFT output image containing aligned myoblast information.

Conclusions

This study was designed to develop the biofunctional scaffolds that can promote cellular behaviors and facilitate the myogenesis. The aligned GO-PLGA/RGD nanofiber sheets were successfully fabricated by MFAES, and their potentials as skeletal tissue engineering scaffolds were investigated. It was shown that the random GO-PLGA/RGD nanofiber sheets had a three-dimensional network structure resembling the natural ECM, while the aligned GO-PLGA/RGD nanofiber sheets had a highly aligned structure. The RGD peptide and GO were uniformly decorated in the sheets, and the physicochemical and mechanical properties of GO-PLGA/RGD nanofiber sheets were suitable for supporting cell growth. In addition, the initial attachment and proliferation of C2C12 skeletal myoblasts were significantly promoted on the GO-PLGA/RGD nanofiber sheets due to the synergistic effects of RGD peptide and GO. Moreover, the GO-PLGA/RGD sheets could accelerate the myogenic differentiation without additional myogenic factors. The myogenic differentiation analysis revealed that the aligned GO-PLGA/RGD nanofiber sheets could not only effectively induce myoblast alignment, but could also favorably stimulate the spontaneous myogenic differentiation. Collectively, it is proposed that the aligned GO-PLGA/RGD nanofiber sheets are one of the most promising approaches for facilitating myogenesis and promoting skeletal tissue regeneration.

Supplementary Material

Supplementary figures and tables.

<http://www.ntno.org/v02p0144s1.pdf>

Acknowledgements

This research was supported by Basic Science Research Program through the National Research Foundation (NRF) of Korea funded by the Ministry of Education (No. 2016R1D1A1B03931076) and Creative Materials Discovery Program through the NRF of Korea funded by Ministry of Science and ICT (NRF-2017M3D1A1039287). Also, this study was supported by a grant of the Korea Health Technology R&D Project through the Korea Health Industry Development Institute (KHIDI) funded by the Ministry of Health & Welfare, Republic of Korea (No. HI17C1662) and the Technology Innovation Program (N0002310) funded by the Ministry of Trade, Industry & Energy (MOTIE, Korea).

Competing Interests

The authors have declared that no competing

interest exists.

References

- Borselli C, Cezar CA, Shvartsman D, et al. The role of multifunctional delivery scaffold in the ability of cultured myoblasts to promote muscle regeneration. *Biomaterials*. 2011; 32: 8905-8914.
- Kwee BJ and Mooney DJ. Biomaterials for skeletal muscle tissue engineering. *Curr Opin Biotechnol*. 2017; 47: 16-22.
- Ege D, Kamali AR and Boccaccini AR. Graphene oxide/polymer-based biomaterials. *Adv Eng Mater*. 2017; 19: 1700627.
- Shin YC, Shin DM, Lee EJ, et al. Hyaluronic acid/PLGA core/shell fiber matrices loaded with EGCG beneficial to diabetic wound healing. *Adv Healthc Mater*. 2016; 5: 3035-3045.
- Lee S-W and Belcher AM. Virus-based fabrication of micro-and nanofibers using electrospinning. *Nano Lett*. 2004; 4: 387-390.
- Wang J, Wang L, Li X, et al. Virus activated artificial ECM induces the osteoblastic differentiation of mesenchymal stem cells without osteogenic supplements. *Sci Rep*. 2013; 3: 1242.
- Mao C, Liu A and Cao B. Virus-Based Chemical and Biological Sensing. *Angew Chem Int Ed*. 2009; 48: 6790-6810.
- He T, Abbineni G, Cao B, et al. Nanofibrous bio-inorganic hybrid structures formed through self-assembly and oriented mineralization of genetically engineered phage nanofibers. *Small*. 2010; 6: 2230-2235.
- Oh J-W, Chung W-J, Heo K, et al. Biomimetic virus-based colourimetric sensors. *Nat Commun*. 2014; 5: 3043.
- Merzlyak A, Indrakanti S and Lee S-W. Genetically engineered nanofiber-like viruses for tissue regenerating materials. *Nano Lett*. 2009; 9: 846-852.
- Chung W-J, Merzlyak A, Yoo SY, et al. Genetically engineered liquid-crystalline viral films for directing neural cell growth. *Langmuir*. 2010; 26: 9885-9890.
- Pytela R, Pierschbacher MD, Ginsberg MH, et al. Platelet membrane glycoprotein IIb/IIIa: member of a family of Arg-Gly-Asp--specific adhesion receptors. *Science*. 1986; 231: 1559-1562.
- Ruoslahti E and Pierschbacher MD. New perspectives in cell adhesion: RGD and integrins. *Science*. 1987; 238: 491-497.
- Zhang Y, Nayak TR, Hong H, et al. Graphene: A versatile nanoplatform for biomedical applications. *Nanoscale*. 2012; 4: 3833-3842.
- Chung C, Kim Y-K, Shin D, et al. Biomedical applications of graphene and graphene oxide. *Accounts Chem Res*. 2013; 46: 2211-2224.
- Ku SH and Park CB. Myoblast differentiation on graphene oxide. *Biomaterials*. 2013; 34: 2017-2023.
- Lee JH, Lee Y, Shin YC, et al. *In situ* forming gelatin/graphene oxide hydrogels for facilitated C2C12 myoblast differentiation. *Appl Spectrosc Rev*. 2016; 51: 527-539.
- Choi JS, Lee SJ, Christ GJ, et al. The influence of electrospun aligned poly(ϵ -caprolactone)/collagen nanofiber meshes on the formation of self-aligned skeletal muscle myotubes. *Biomaterials*. 2008; 29: 2899-2906.
- Cooper A, Jana S, Bhattarai N, et al. Aligned chitosan-based nanofibers for enhanced myogenesis. *J Mat Chem*. 2010; 20: 8904-8911.
- Dang JM and Leong KW. Myogenic induction of aligned mesenchymal stem cell sheets by culture on thermally responsive electrospun nanofibers. *Adv Mater*. 2007; 19: 2775-2779.
- Ku SH, Lee SH and Park CB. Synergic effects of nanofiber alignment and electroactivity on myoblast differentiation. *Biomaterials*. 2012; 33: 6098-6104.
- Lam MT, Sim S, Zhu X, et al. The effect of continuous wavy micropatterns on silicone substrates on the alignment of skeletal muscle myoblasts and myotubes. *Biomaterials*. 2006; 27: 4340-4347.
- Shin YC, Lee JH, Jin L, et al. Cell-adhesive RGD peptide-displaying M13 bacteriophage/PLGA nanofiber matrices for growth of fibroblasts. *Biomater Res*. 2014; 18: 14.
- Shin YC, Lee JH, Kim MJ, et al. Biomimetic hybrid nanofiber sheets composed of RGD peptide-decorated PLGA as cell-adhesive substrates. *J Funct Biomater*. 2015; 6: 367-378.
- Shin YC, Lee JH, Jin L, et al. Cell-adhesive matrices composed of RGD peptide-displaying M13 bacteriophage/poly(lactic-co-glycolic acid) nanofibers beneficial to myoblast differentiation. *J Nanosci Nanotechnol*. 2015; 15: 7907-7912.
- Hummers Jr WS and Offeman RE. Preparation of graphitic oxide. *J Am Chem Soc*. 1958; 80: 1339-1339.
- Li D, Wang Y and Xia Y. Electrospinning of polymeric and ceramic nanofibers as uniaxially aligned arrays. *Nano Lett*. 2003; 3: 1167-1171.
- Katta P, Alessandro M, Ramsier RD, et al. Continuous electrospinning of aligned polymer nanofibers onto a wire drum collector. *Nano Lett*. 2004; 4: 2215-2218.
- Liu Y, Zhang X, Xia Y, et al. Magnetic-field-assisted electrospinning of aligned straight and wavy polymeric nanofibers. *Adv Mater*. 2010; 22: 2454-2457.
- Ayres C, Bowlin GL, Henderson SC, et al. Modulation of anisotropy in electrospun tissue-engineering scaffolds: Analysis of fiber alignment by the fast Fourier transform. *Biomaterials*. 2006; 27: 5524-5534.
- Ayres CE, Bowlin GL, Pizinger R, et al. Incremental changes in anisotropy induce incremental changes in the material properties of electrospun scaffolds. *Acta Biomater*. 2007; 3: 651-661.

32. McClure MJ, Sell SA, Ayres CE, et al. Electrospinning-aligned and random poly(dioxanone–polycaprolactone–silk fibroin-blended scaffolds: geometry for a vascular matrix. *Biomed Mater.* 2009; 4: 055010.
33. McClure MJ, Garg K, Simpson DG, et al. The influence of platelet-rich plasma on myogenic differentiation. *J Tissue Eng Regen Med.* 2016; 10: E239–E249.
34. Atabaev TS, Jin OS, Lee JH, et al. Facile synthesis of bifunctional silica-coated core-shell $Y_2O_3:Eu^{3+},Co^{2+}$ composite particles for biomedical applications. *RSC Adv.* 2012; 2: 9495-9501.
35. Lee JH, Shin YC, Jin OS, et al. Enhanced neurite outgrowth of PC-12 cells on graphene-monolayer-coated substrates as biomimetic cues. *J Korean Phys Soc.* 2012; 61: 1696-1699.
36. Majewska A, Yiu G and Yuste R. A custom-made two-photon microscope and deconvolution system. *Pflügers Arch Eur J Phys.* 2000; 441: 398-408.
37. Kim MJ, Shin YC, Lee JH, et al. Multiphoton imaging of myogenic differentiation in gelatin-based hydrogels as tissue engineering scaffolds. *Biomater Res.* 2016; 20: 2.
38. Liu F, Guo R, Shen M, et al. Effect of processing variables on the morphology of electrospun poly [(lactic acid)-co-(glycolic acid)] nanofibers. *Macromol Mater Eng.* 2009; 294: 666-672.
39. Deitzel JM, Kleinmeyer J, Harris DEA, et al. The effect of processing variables on the morphology of electrospun nanofibers and textiles. *Polymer.* 2001; 42: 261-272.
40. Wang Z, Zhao Y, Luo Y, et al. Attapulgite-doped electrospun poly (lactic-co-glycolic acid) nanofibers enable enhanced osteogenic differentiation of human mesenchymal stem cells. *RSC Adv.* 2015; 5: 2383-2391.
41. Shin YC, Lee JH, Jin L, et al. Stimulated myoblast differentiation on graphene oxide-impregnated PLGA-collagen hybrid fibre matrices. *J Nanobiotechnol.* 2015; 13: 21.
42. You MH, Kwak MK, Kim DH, et al. Synergistically enhanced osteogenic differentiation of human mesenchymal stem cells by culture on nanostructured surfaces with induction media. *Biomacromolecules.* 2010; 11: 1856-1862.
43. Wang X, Ding B and Li B. Biomimetic electrospun nanofibrous structures for tissue engineering. *Mater Today.* 2013; 16: 229-241.
44. Xu T, Miszuk JM, Zhao Y, et al. Electrospun polycaprolactone 3D nanofibrous scaffold with interconnected and hierarchically structured pores for bone tissue engineering. *Adv Healthc Mater.* 2015; 4: 2238-2246.
45. Yoon OJ, Jung CY, Sohn IY, et al. Nanocomposite nanofibers of poly (D, L-lactic-co-glycolic acid) and graphene oxide nanosheets. *Compos A Appl Sci Manuf.* 2011; 42: 1978-1984.
46. Kim CH, Khil MS, Kim HY, et al. An improved hydrophilicity via electrospinning for enhanced cell attachment and proliferation. *J Biomed Mater Res B.* 2006; 78: 283-290.
47. Shin YC, Jin L, Lee JH, et al. Graphene oxide-incorporated PLGA-collagen fibrous matrices as biomimetic scaffolds for vascular smooth muscle cells. *Sci Adv Mater.* 2017; 9: 232-237.
48. van Apeldoorn AA, Van Manen H-J, Bezemer JM, et al. Raman imaging of PLGA microsphere degradation inside macrophages. *J Am Chem Soc.* 2004; 126: 13226-13227.
49. Zhu G, Zhu X, Fan Q, et al. Raman spectra of amino acids and their aqueous solutions. *Spectrosc Acta Pt A-Molec Biomolec Spectr.* 2011; 78: 1187-1195.
50. Kudin KN, Ozbas B, Schniepp HC, et al. Raman spectra of graphite oxide and functionalized graphene sheets. *Nano Lett.* 2008; 8: 36-41.
51. Maiti NC, Apetri MM, Zagorski MG, et al. Raman spectroscopic characterization of secondary structure in natively unfolded proteins: α -synuclein. *J Am Chem Soc.* 2004; 126: 2399-2408.
52. Stewart S and Fredericks PM. Surface-enhanced Raman spectroscopy of amino acids adsorbed on an electrochemically prepared silver surface. *Spectrosc Acta Pt A-Molec Biomolec Spectr.* 1999; 55: 1641-1660.
53. Lee EJ, Lee JH, Jin L, et al. Hyaluronic acid/poly (lactic-co-glycolic acid) core/shell fiber meshes loaded with epigallocatechin-3-O-gallate as skin tissue engineering scaffolds. *J Nanosci Nanotechnol.* 2014; 14: 8458-8463.
54. Donovan DL, Schmidt SP, Townshend SP, et al. Material and structural characterization of human saphenous vein. *J Vasc Surg.* 1990; 12: 531-537.
55. Yoon OJ, Sohn IY, Kim DJ, et al. Enhancement of thermomechanical properties of poly (D, L-lactic-co-glycolic acid) and graphene oxide composite films for scaffolds. *Macromol Res.* 2012; 20: 789-794.
56. Full SM, Delman C, Gluck JM, et al. Effect of fiber orientation of collagen-based electrospun meshes on human fibroblasts for ligament tissue engineering applications. *J Biomed Mater Res B.* 2015; 103: 39-46.
57. Baek HS, Yoo JY, Rah DK, et al. Evaluation of the extraction method for the cytotoxicity testing of latex gloves. *Yonsei Med J.* 2005; 46: 579-583.
58. Huang T and Zheng Y. Uniform and accelerated degradation of pure iron patterned by Pt disc arrays. *Sci Rep.* 2016; 6.
59. Kuo Z-K, Lai P-L, Toh EK-W, et al. Osteogenic differentiation of preosteoblasts on a hemostatic gelatin sponge. *Sci Rep.* 2016; 6: 32884.
60. Hersel U, Dahmen C and Kessler H. RGD modified polymers: biomaterials for stimulated cell adhesion and beyond. *Biomaterials.* 2003; 24: 4385-4415.
61. Bellis SL. Advantages of RGD peptides for directing cell association with biomaterials. *Biomaterials.* 2011; 32: 4205-4210.
62. Yi J, Xiong F, Li B, et al. Degradation characteristics, cell viability and host tissue responses of PDLA-based scaffold with PRGD and β -TCP nanoparticles incorporation. *Regen Biomater.* 2016; 3: 159-166.
63. Shin YM, Jo SY, Park JS, et al. Synergistic effect of dual-functionalized fibrous scaffold with BCP and RGD containing peptide for improved osteogenic differentiation. *Macromol Biosci.* 2014; 14: 1190-1198.
64. Lee WC, Lim CHY, Shi H, et al. Origin of enhanced stem cell growth and differentiation on graphene and graphene oxide. *ACS nano.* 2011; 5: 7334-7341.
65. Shin YC, Kim J, Kim SE, et al. RGD peptide and graphene oxide co-functionalized PLGA nanofiber scaffolds for vascular tissue engineering. *Regen Biomater.* 2017; 4: 159-166.
66. Shin YC, Lee JH, Kim MJ, et al. Stimulating effect of graphene oxide on myogenesis of C2C12 myoblasts on RGD peptide-decorated PLGA nanofiber matrices. *J Biol Eng.* 2015; 9: 22.
67. Zhao G, Schwartz Z, Wieland M, et al. High surface energy enhances cell response to titanium substrate microstructure. *J Biomed Mater Res A.* 2005; 74: 49-58.
68. Shin YC, Lee JH, Jin OS, et al. RGD peptide-displaying M13 bacteriophage/PLGA nanofibers as cell-adhesive matrices for smooth muscle cells. *J Korean Phys Soc.* 2015; 66: 12-16.
69. Redfield A, Nieman MT and Knudsen KA. Cadherins promote skeletal muscle differentiation in three-dimensional cultures. *J Cell Biol.* 1997; 138: 1323-1331.
70. Olson EN. Interplay between proliferation and differentiation within the myogenic lineage. *Dev Biol.* 1992; 154: 261-272.
71. Brennan TJ and Olson EN. Myogenin resides in the nucleus and acquires high affinity for a conserved enhancer element on heterodimerization. *Genes Dev.* 1990; 4: 582-595.
72. Chandran R, Knobloch TJ, Anghelina M, et al. Biomechanical signals upregulate myogenic gene induction in the presence or absence of inflammation. *Am J Physiol Cell Physiol.* 2007; 293: C267-C276.
73. Grinou A, Yun YS and Jin H-J. Polyaniline nanofiber-coated polystyrene/graphene oxide core-shell microsphere composites. *Macromol Res.* 2012; 20: 84-92.
74. Nayak TR, Andersen H, Makam VS, et al. Graphene for controlled and accelerated osteogenic differentiation of human mesenchymal stem cells. *ACS nano.* 2011; 5: 4670-4678.
75. Park SY, Park J, Sim SH, et al. Enhanced differentiation of human neural stem cells into neurons on graphene. *Adv Mater.* 2011; 23: H263-H267.
76. Lee T-J, Park S, Bhang SH, et al. Graphene enhances the cardiomyogenic differentiation of human embryonic stem cells. *Biochem Biophys Res Commun.* 2014; 452: 174-180.
77. Chen G-Y, Pang D-P, Hwang S-M, et al. A graphene-based platform for induced pluripotent stem cells culture and differentiation. *Biomaterials.* 2012; 33: 418-427.
78. Chen M-C, Sun Y-C and Chen Y-H. Electrically conductive nanofibers with highly oriented structures and their potential application in skeletal muscle tissue engineering. *Acta Biomater.* 2013; 9: 5562-5572.
79. Clark P, Dunn G, Knibbs A, et al. Alignment of myoblasts on ultrafine gratings inhibits fusion in vitro. *Int J Biochem Cell Biol.* 2002; 34: 816-825.
80. Yamamoto DL, Csikasz RI, Li Y, et al. Myotube formation on micro-patterned glass: intracellular organization and protein distribution in C2C12 skeletal muscle cells. *J Histochem Cytochem.* 2008; 56: 881-892.
81. Dugan JM, Gough JE and Eichhorn SJ. Directing the morphology and differentiation of skeletal muscle cells using oriented cellulose nanowhiskers. *Biomacromolecules.* 2010; 11: 2498-2504.
82. Perry RL and Rudnick MA. Molecular mechanisms regulating myogenic determination and differentiation. *Front Biosci.* 2000; 5: D750-767.
83. Patel S, Kurpinski K, Quigley R, et al. Bioactive nanofibers: synergistic effects of nanotopography and chemical signaling on cell guidance. *Nano Lett.* 2007; 7: 2122-2128.